engineering proceedings

MDPI

Proceeding Paper

Coupled Temperature–Porosity Effects on Nonlinear Bending Behavior of Functionally Graded Porous Sandwich Frames †

Thanh Tien Pham [1,2,*], Dinh Kien Nguyen [1,3] and Cong Ich Le [4]

[1] Institute of Mechanics, Vietnam Academy of Science and Technology (VAST), 18 Hoang Quoc Viet, Hanoi 10072, Vietnam; ndkien@imech.vast.vn
[2] Graduate University of Science and Technology, Vietnam Academy of Science and Technology (VAST), 18 Hoang Quoc Viet, Hanoi 10072, Vietnam
[3] Faculty of Mechanical Engineering, Thuyloi University, 175 Tay Son, Kim Lien Ward, Hanoi 11520, Vietnam
[4] Faculty of Mechanical Engineering, Le Quy Don Technical University, 236 Hoang Quoc Viet, Hanoi 11307, Vietnam; lecongich79@lqdtu.edu.vn
* Correspondence: iamptien@gmail.com
† Presented at the 2026 International Conference on Energy, Infrastructure and Environmental Research (EIER 2026), Ho Chi Minh City, Vietnam, 15–17 July 2026.

Abstract

This study develops an efficient finite formulation to predict thermoelastic nonlinear bending of sandwich frames with a functionally graded porous (FGP) core and homogeneous face sheets. The formulation incorporates temperature-dependent properties and various thickness-graded porosity patterns, utilizing third-order shear deformation theory and von Kármán nonlinear relations. To enhance computational efficiency, the model employs shear rotation as the independent variable rather than traditional cross-sectional rotation. Nonlinear equations are solved using the Newton–Raphson method. Results demonstrate a significant impact of thermal and porosity effects on the nonlinear response, and the frame deformation is significantly increased when increasing the porosity coefficient and temperature. Detailed analysis is presented to show the effects of porosity coefficients, distribution patterns, and temperature increments on the frame nonlinear behavior.

Keywords: porous sandwich frame; thermal effect; nonlinear bending; finite element analysis

1. Introduction

Functionally graded porous (FGP) materials have emerged as a promising solution for modern lightweight structures, offering the ability to customize thermoelastic properties by tailoring internal pore distributions. Recently, these materials have been integrated into frames—the most prevalent load-bearing systems—to minimize total weight and enhance thermal resistance [1]. From an engineering perspective, frames typically consist of slender members that undergo significant deformation under load. Consequently, nonlinear analysis of FGP frames under thermomechanical loading is essential for the robust design of these structures.

Various theories can be employed to model frame deformation, among which Third-order Shear Deformation Theory (TSDT) is often preferred as it eliminates the need for shear correction factors. Utilizing TSDT within a finite element framework—combined with a strategic selection of independent variables—effectively mitigates the shear-locking phenomenon, a common deficiency in first-order theory-based formulations [2]. Regarding the FGP beam and frame structures, most current studies focus on single beams or consider temperature-independent material properties [3,4].

Check for updates

Academic Editor: Huynh Anh Duy Nguyen

Published: 11 November 2026

Copyright: © 2026 by the authors. Licensee MDPI, Basel, Switzerland. This article is an open access article distributed under the terms and conditions of the Creative Commons Attribution (CC BY) license.

Despite the growing interest in porous sandwich beam and frame structures, studies addressing geometrically nonlinear responses of porous sandwich frames with temperature-dependent material properties remain very limited. To fill this gap, this paper presents an efficient finite element formulation for predicting the nonlinear bending responses of porous sandwich frames, accounting for thermal dependence of material properties and different porosity distribution patterns. Based on a third-order shear deformation theory and von Kármán nonlinear relationship, the formulation is derived using transverse shear rotation as an independent variable. The resulting discretized nonlinear equilibrium equation is established and solved by the Newton–Raphson iterative procedure. A parametric study is conducted to show the efficiency of the proposed formulation and to highlight the influence of key governing factors on the nonlinear behavior of the frames.

2. Mathematical Formulation

Figure 1 shows a beam element with length L, width b, and thickness h in both local and global coordinate systems. The element consists of a porous core sandwiched between two face sheets. Three porosity distribution patterns in the thickness, namely symmetric, asymmetric, and uniform, are considered. The material properties are considered to be temperature-dependent, and a typical property varies with temperature T according to [1,5]

$$P(T) = P_0\left(P_{-1}T^{-1} + 1 + P_1T^1 + P_2T^2 + P_3T^3\right) \tag{1}$$

where $T = T_0 + \Delta T$ with $T_0 = 300°$ K is the reference temperature; P_{-1}, P_0, P_1, P_2, and P_3 are material-specific temperature coefficients.

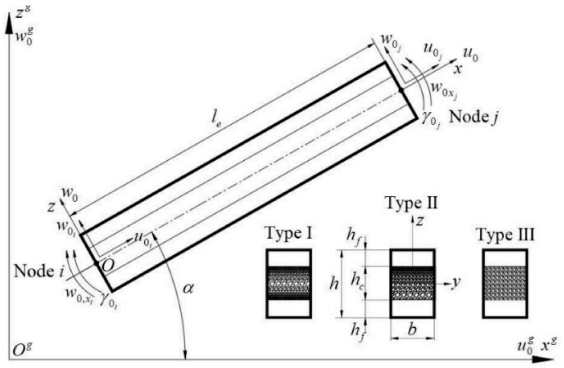


Figure 1. Geometry and kinematics of an FGP beam element.

The effective Young's modulus (E), thermal expansion coefficient (λ), and shear modulus (G) of the porous core are dependent on the three porous distribution patterns as follows [1]:

Type I: Symmetric distribution

$$\begin{gathered} E(z,T) = E_1(T)\left[1 - e_0\cos\left(\pi\tfrac{z}{h_c}\right)\right],\ \lambda(z,T) = \lambda_1(T)\left[1 - e_0\cos\left(\pi\tfrac{z}{h_c}\right)\right], \\ G(z,T) = G_1(T)\left[1 - e_0\cos\left(\pi\tfrac{z}{h_c}\right)\right],\ \text{for}\ -\tfrac{h_c}{2} \le z \le \tfrac{h_c}{2} \end{gathered} \tag{2}$$

Type II: Asymmetric distribution

$$\begin{gathered} E(z,T) = E_1(T)\left[1 - e_0\cos\left(\tfrac{\pi}{2}\tfrac{z}{h_c} + \tfrac{\pi}{4}\right)\right],\ \lambda(z,T) = \lambda_1(T)\left[1 - e_0\cos\left(\tfrac{\pi}{2}\tfrac{z}{h_c} + \tfrac{\pi}{4}\right)\right], \\ G(z,T) = G_1(T)\left[1 - e_0\cos\left(\tfrac{\pi}{2}\tfrac{z}{h_c} + \tfrac{\pi}{4}\right)\right],\ \text{for}\ -\tfrac{h_c}{2} \le z \le \tfrac{h_c}{2} \end{gathered} \tag{3}$$

Type III: Uniform distribution

$$\begin{gathered} E(z,T) = E_1(T)[1 - e_0a],\ \lambda(z,T) = \lambda_1(T)[1 - e_0a], \\ G(z,T) = G_1(T)[1 - e_0a],\ \text{for}\ -h_c/2 \le z \le h_c/2 \end{gathered} \tag{4}$$

https://doi.org/10.3390/engproc2026164002

Both the top and bottom face sheets consist of pure isotropic materials with properties determined by the Young modulus and shear modulus

$$E(z,T) = E_1,\ G(z,T) = G_1,\ \text{for}\ -h_c \le z \le h_c \text{ and } -h_c \le z \le h_c \tag{5}$$

For a uniform porosity distribution, the core properties are constant through the thickness, and the coefficient a in Equation (4) is given by

$$a = \frac{1}{e_0} - \frac{1}{e_0}\left(\frac{2}{\pi}\sqrt{1-e_0} - \frac{2}{\pi} + 1\right)^2 \tag{6}$$

According to the third-order shear deformation theory [6], the displacement components in the x and z directions of a point within the element are expressed as follows

$$u(x,z) = u_0(x) - z\,\theta_0(x,t) - \frac{4z^3}{3h^2}\left[w_{0,x}(x) - \theta_0(x)\right],\ w(x,z) = w_0(x) \tag{7}$$

The variables u_0 and w_0 denote the axial and transverse displacements of a point on the mid-plane, respectively, while θ_0 represents the cross-sectional rotation. The subscript comma in Equation (7) and below indicates the partial derivative, e.g., $(\cdot)_{,x} = \partial(\cdot)/\partial \mathrm{x}$. Following Shi and Lam [2], the finite element formulation is more efficient by adopting the following transverse shear rotation as an independent variable

$$\gamma_0(x) = w_{0,x}(x) - \theta_0(x) \tag{8}$$

Using the transverse shear rotation γ_0, one can recast the displacements in Equation (7) in the form

$$u(x,z) = u_0 - z\,(w_{0,x} - \gamma_0) - \frac{4z^3}{3h^2}\,\gamma_0,\ w(x,z) = w_0 \tag{9}$$

Let u_0^g, w_0^g and γ_0^g be the global displacements in the x_g-, z_g-directions, and the global transverse shear deformation, respectively. The local displacements and rotation are related to the global ones by

$$\begin{Bmatrix} u_0 \\ w_0 \\ \gamma_0 \end{Bmatrix} = \begin{bmatrix} c & s & 0 \\ -s & c & 0 \\ 0 & 0 & 1 \end{bmatrix} \begin{Bmatrix} u_0^g \\ w_0^g \\ \gamma_0^g \end{Bmatrix} \tag{10}$$

with

$$c = \cos\alpha,\ s = \sin\alpha \tag{11}$$

Equation (9) gives the strains in term of von Kármán nonlinear relation in the form

$$\begin{aligned} \varepsilon_{xx} &= u_{,x} + \tfrac{1}{2}w_{,x}^2 = u_{0,x} + \tfrac{1}{2}w_{0,x}^2 - z\,(w_{0,xx} - \gamma_{,x}) - \tfrac{4z^3}{3h^2}\gamma_{,x} \\ &= \varepsilon_0 - z\,(w_{0,xx} - \gamma_{0,x}) - \tfrac{4z^3}{3h^2}\gamma_{0,x},\ \gamma_{xz} = u_{,z} + w_{,x} = \gamma_0\left(1 - \tfrac{4z^2}{h^2}\right) \end{aligned} \tag{12}$$

where $\varepsilon_0 = u_{0,x} + \frac{1}{2}w_{0,x}^2$ is the membrane strain.

Based on Hooke's law, the constitutive relations for the stresses σ_{xx} and τ_{xz} are given by

$$\begin{Bmatrix} \sigma_{xx} \\ \tau_{xz} \end{Bmatrix} = \begin{bmatrix} E(z,T) & 0 \\ 0 & G(z,T) \end{bmatrix} \begin{Bmatrix} \varepsilon_{xx} \\ \gamma_{xz} \end{Bmatrix} \tag{13}$$

where $E(z,T)$ and $G(z,T)$ are defined by Equations (2)–(4).

The elastic strain energy of the sandwich beam reads

$$U^e = \frac{1}{2}\int_{V^e} (\sigma_{xx}\varepsilon_{xx} + \tau_{xz}\gamma_{xz})\mathrm{d}V \tag{14}$$

where V^e is the volume of the beam element.

https://doi.org/10.3390/engproc2026164002

Using Equations (12) and (13), one can write the strain energy in Equation (14) in the form

$$U^e = \frac{1}{2}\int_0^{l_e} \left\{I_1\varepsilon_0^2 + I_2(w_{0,xx} - \gamma_{0,x})^2 + 2I_3(w_{0,xx} - \gamma_{0,x})\gamma_{0,x} + I_4\gamma_{0,x}^2 + I_5\gamma_0^2\right\}\mathrm{d}x \tag{15}$$

with I_i $(i = 1,\ldots,5)$ being the rigidities, defined as

$$\begin{aligned}\{I_1,\ I_2,\ I_3,\ I_4\} &= b\sum_{i=1}^{3}\int_{h_{i-1}}^{h_i} E(z,T)\left\{1, z^2, \frac{4z^4}{3h^2}, \frac{16z^6}{9h^4}\right\}\mathrm{d}z,\\ I_5 &= b\sum_{i=1}^{3}\int_{h_{i-1}}^{h_i} G(z,T)\left(1 - \frac{4z^2}{h^2}\right)\mathrm{d}z\end{aligned} \tag{16}$$

where $h_0 = -h/2,\ h_1 = -h_c/2,\ h_2 = h_c/2,\ h_3 = h/2$.

The thermal strain energy due to temperature rise is given by [5]

$$U_T^e = \frac{1}{2}\int_0^{l_e} N_T w_{0,x}^2\mathrm{d}x \tag{17}$$

where N_T is the thermal resultant, which can be expressed as

$$N_T(z,T) = -\int_A E(z,T)\lambda(z,T)\Delta T\mathrm{d}A \tag{18}$$

with λ as the thermal expansion coefficient defined in Equations (2)–(4).

The work done by the external loads is given by

$$W_{ex}^e = \int_0^{l_e} w(x)q(x)\mathrm{d}x \tag{19}$$

where $q(x)$ denotes the distributed load, with a concentrated load treated as a special case.

The nonlinear equilibrium equations are derived from the principle of virtual work as follows.

$$\sum^{\mathrm{nELE}}\left(\delta U^e + \delta U_T^e - \delta W_{ex}^e\right) = 0 \tag{20}$$

where nELE is the total number of elements. Equation (20) leads to a system of nonlinear differential equations with unknowns u_0, w_0, and γ_0. Due to its complexity, the finite element method is used herein to construct the discretized equilibrium equations and to predict the bending response.

3. Solution Method

A two-node beam element is considered. The local vector of degrees of freedom (d.o.f.) for the element, $\boldsymbol{\Delta}_e$, contains the displacements and shear rotations at the two nodes with the form

$$\boldsymbol{\Delta}_e = \left\{\mathbf{u}_0,\ \mathbf{w}_0,\ \boldsymbol{\gamma}_0\right\}^T \tag{21}$$

in which

$$\mathbf{u}_0 = \left\{u_{0_1},\ u_{0_2}\right\}^T,\ \mathbf{w}_0 = \left\{w_{0_1},\ w_{0x_1},\ w_{0_2},\ w_{0x_2}\right\}^T,\ \boldsymbol{\gamma}_0 = \left\{\gamma_{0_1},\ \gamma_{0_2}\right\}^T \tag{22}$$

are the vectors, the local axial displacements and the shear rotations at the nodes as depicted in Figure 1. The superscript "T" in the above equation and below indicates the transpose of vector or a matrix. The displacements and shear deformation inside the element are interpolated as [7]

$$u_0 = \mathbf{h}\mathbf{u}_0,\ w_0 = \mathbf{h}_w\mathbf{w}_0,\ \gamma_0 = \mathbf{h}\,\boldsymbol{\gamma}_0 \tag{23}$$

with $\mathbf{h}$ as the matrix of linear functions and $\mathbf{h}_w$ as the matrix of cubic polynomials, and they have the following forms [7]

$$\mathbf{h} = \left\{1 - \frac{x}{l_e},\ \frac{x}{l_e}\right\},\ \mathbf{h}_w = \left\{1 - \frac{3x^2}{l_e^2} + \frac{2x^3}{l_e^3},\ x - \frac{2x^2}{l_e} + \frac{x^3}{l_e^2},\ \frac{3x^2}{l_e^2} - \frac{2x^3}{l_e^3},\ -\frac{x^2}{l_e} + \frac{x^3}{l_e^2}\right\} \tag{24}$$

Taking the derivative of Equation (23) with respect to x, we obtain

$$u_{0,x} = \mathbf{h}_{,x}\,\mathbf{u}_0,\ w_{0,x} = \mathbf{h}_{w,x}\mathbf{w}_0,\ w_{0,xx} = \mathbf{h}_{w,xx}\mathbf{w}_0,\ \gamma_{0,x} = \mathbf{h}_{,x}\,\boldsymbol{\gamma}_0 \tag{25}$$

The axial strain in Equation (12) and the interpolation (24), (25) may cause membrane locking in the finite element. To overcome this, the membrane strain ε_0 is replaced by an effective strain, as proposed in [7]

$$\varepsilon_{\text{eff.}} = \frac{1}{l_e}\int_0^{l_e} \varepsilon_0 \mathrm{d}x = \frac{1}{l_e}\int_0^{l_e} \left(u_{0,x} + \frac{1}{2}w_{0,x}^2\right)\mathrm{d}x = \frac{1}{l_e}\int_0^{l_e} \left(\mathbf{h}_{,x}\mathbf{u}_0 + \frac{1}{2}(\mathbf{h}_{w,x}\mathbf{w}_0)^2\right)\mathrm{d}x \tag{26}$$

From Equations (24) and (25), one can write Equation (26) in the form

$$\varepsilon_{\text{eff.}} = \mathbf{b}_1\mathbf{u}_0 + \mathbf{w}_0^T\mathbf{B}_1\,\mathbf{w}_0 \tag{27}$$

where

$$\mathbf{b}_1 = \int_0^{l_e} \mathbf{h}_{,x}\mathrm{d}x,\ \mathbf{B}_1 = \frac{1}{2l_e}\int_0^{l_e} \mathbf{h}_{w,x}^T\mathbf{h}_{w,x}dx \tag{28}$$

With the interpolations, the strain energy in Equation (15) can be expressed in matrix form as

$$\begin{aligned} U^e = \tfrac{1}{2}\Big\{ & l_e I_1(\mathbf{b}_1\mathbf{u}_0 + \mathbf{w}_0^T\mathbf{B}_1\mathbf{w}_0)^2 + I_2(\mathbf{w}_0^T\mathbf{B}_2\mathbf{w}_0 - 2\mathbf{w}_0^T\mathbf{B}_3\gamma_0 + \gamma_0^T\mathbf{B}_4\gamma_0) \\ & + 2I_3(\mathbf{w}_0^T\mathbf{B}_3\gamma_0 - \gamma_0^T\mathbf{B}_4\gamma_0) + I_4(\gamma_0^T\mathbf{B}_4\gamma_0) + I_5(\gamma_0^T\mathbf{B}_5\gamma_0)\Big\} \end{aligned} \tag{29}$$

where

$$\mathbf{B}_2 = \int_0^{l_e} \mathbf{h}_{w,xx}^T\mathbf{h}_{w,xx}\mathrm{d}x,\ \mathbf{B}_3 = \int_0^{l_e} \mathbf{h}_{w,xx}^T\mathbf{h}_{,x}\mathrm{d}x,\ \mathbf{B}_4 = \int_0^{l_e} \mathbf{h}_{,x}^T\mathbf{h}_{,x}dx,\ \mathbf{B}_5 = \int_0^{l_e} \mathbf{h}^T\mathbf{h}dx \tag{30}$$

and

$$U_T^e = \frac{1}{2}\int_0^{l_e} N_T(\mathbf{h}_{w,x}\mathbf{w}_0)^2 dx = \frac{1}{2}\mathbf{w}_0^T\left[\int_0^{l_e} N_T\mathbf{h}_{w,x}^T\mathbf{h}_{w,x}dx\right]\mathbf{w}_0 = l_e N_T\mathbf{w}_0^T\mathbf{B}_1\mathbf{w}_0 \tag{31}$$

Therefore,

$$\begin{aligned} U_{total}^e = \tfrac{1}{2}\Big\{ & l_e I_1(\mathbf{b}_1\mathbf{u}_0 + \mathbf{w}_0^T\mathbf{B}_1\,\mathbf{w}_0)^2 + I_2(\mathbf{w}_0^T\mathbf{B}_2\mathbf{w}_0 - 2\mathbf{w}_0^T\mathbf{B}_3\boldsymbol{\gamma}_0 + \boldsymbol{\gamma}_0^T\mathbf{B}_4\boldsymbol{\gamma}_0) \\ & + 2I_3(\mathbf{w}_0^T\mathbf{B}_3\boldsymbol{\gamma}_0 - \boldsymbol{\gamma}_0^T\mathbf{B}_4\boldsymbol{\gamma}_0) + I_4(\boldsymbol{\gamma}_0^T\mathbf{B}_4\boldsymbol{\gamma}_0) + I_5(\boldsymbol{\gamma}_0^T\mathbf{B}_5\boldsymbol{\gamma}_0)\Big\} + l_e N_T\mathbf{w}_0^T\mathbf{B}_1\mathbf{w}_0 \end{aligned} \tag{32}$$

The work done by external forces, Equation (19), can be rewritten as follows

$$W_{ex}^e = \int_0^{l_e} (\mathbf{h}_w\mathbf{w}_0)q(x)\mathrm{d}x \tag{33}$$

The internal force vector $\mathbf{f}_{in}^e$ is obtained by differentiating the strain energy Equation (32) with respect to the nodal displacements as follows

$$f_{in}^e = \frac{\partial U_{total}^e}{\partial \Delta_e} = \left\{f_{in}^u,\ \ f_{in}^w,\ \ f_{in}^\gamma\right\}^T \tag{34}$$

in which

$$\underset{(2\times1)}{\mathbf{f}_{\text{in}}^u} = \frac{\partial U_{total}^e}{\partial \mathbf{u}_0},\ \underset{(4\times1)}{\mathbf{f}_{\text{in}}^w} = \frac{\partial U_{total}^e}{\partial \mathbf{w}_0},\ \underset{(2\times1)}{\mathbf{f}_{\text{in}}^\gamma} = \frac{\partial U_{total}^e}{\partial \boldsymbol{\gamma}_0} \tag{35}$$

The external forces element vector, $\mathbf{f}_{ex}^e$, can also be expressed in matrix form as follows

$$\underset{(8\times1)}{\mathbf{f}_{ex}^e} = \left\{0,\ 0,\ \int_0^{l_e} \mathbf{h}_w^T q(x)\mathrm{d}x,\ 0,\ 0\right\}^T \tag{36}$$

https://doi.org/10.3390/engproc2026164002

The local vectors of d.o.f., as well as the internal and external force vectors, are connected to their global counterparts via a transformation matrix transpose; for example

$$\boldsymbol{\Delta}_e = \mathbf{T}_t \boldsymbol{\Delta}_e^g \tag{37}$$

with $\mathbf{T}_t$ being the transformation matrix of size (8×8), and its form can be derived from Equation (11).

By assembling the derived element vectors $\mathbf{f}_{in}^e$ and $\mathbf{f}_{ex}^e$ over all elements, the equilibrium equation can be constructed in the following form [8].

$$\mathbf{R}^g(\mathbf{D}^g, \mathbf{F}_{ex}^g) = \mathbf{F}_{ex}^g - \mathbf{F}_{in}^g(\mathbf{D}^g) = 0 \tag{38}$$

Here, $\mathbf{D}^g$ represents the global vector of d.o.f., while $\mathbf{F}_{ex}^g$, $\mathbf{F}_{in}^g$, and $\mathbf{R}^g$ are the global vectors of external force, internal force, and residual force, respectively.

The global tangent stiffness matrix $\mathbf{K}_t^g$ is derived from the variation in the global internal force, as expressed below

$$\mathbf{K}_t^g(\mathbf{D}^g) = \frac{\partial \mathbf{F}_{in}^g(\mathbf{D}^g)}{\partial \mathbf{D}^g} \tag{39}$$

The global internal force vector and the tangent stiffness matrix are assembled from their respective element-level contributions according to the relationships defined in Equations (10) and (37), as follows

$$\mathbf{F}_{in}^g = \sum^{\text{nELE}} \mathbf{T}_t^T \mathbf{f}_{in}^e, \; \mathbf{K}_t^g = \sum^{\text{nELE}} \mathbf{T}_t^T \mathbf{k}_t^e \mathbf{T}_t \tag{40}$$

Consequently, the element tangent stiffness matrix may be expressed in matrix form as follows

$$\underset{(8\times8)}{\mathbf{k}_t^e} = \frac{\partial \mathbf{f}_{in}^e}{\partial \boldsymbol{\Delta}_e} = \begin{bmatrix} \mathbf{k}_t^{uu} & \mathbf{k}_t^{uw} & \mathbf{0} \\ (\mathbf{k}_t^{uw})^T & \mathbf{k}_t^{ww} & \mathbf{k}_t^{w\gamma} \\ \mathbf{0} & (\mathbf{k}_t^{w\gamma})^T & \mathbf{k}_t^{\gamma\gamma} \end{bmatrix} \tag{41}$$

The submatrices in the above equation are defined as follows

$$\underset{(2\times2)}{\mathbf{k}_t^{uu}} = \frac{\partial \mathbf{f}_{in}^u}{\partial \mathbf{u}_0}, \; \underset{(2\times4)}{\mathbf{k}_t^{uw}} = \frac{\partial \mathbf{f}_{in}^u}{\partial \mathbf{w}_0}, \; \underset{(4\times4)}{\mathbf{k}_t^{ww}} = \frac{\partial \mathbf{f}_{in}^w}{\partial \mathbf{w}_0}, \; \underset{(4\times2)}{\mathbf{k}_t^{w\gamma}} = \frac{\partial \mathbf{f}_{in}^w}{\partial \boldsymbol{\gamma}_0} \underset{(2\times2)}{\mathbf{k}_t^{\gamma\gamma}} = \frac{\partial \mathbf{f}_{in}^\gamma}{\partial \boldsymbol{\gamma}_0} \tag{42}$$

The global tangent stiffness is then employed in the following linearized equilibrium equation

$$\mathbf{K}_t^g(\mathbf{D}^g)\delta\mathbf{D}^g = \mathbf{R}^g(\mathbf{D}^g, \mathbf{F}_{ex}^g) = \mathbf{F}_{ex}^g - \mathbf{F}_{in}^g(\mathbf{D}^g) \tag{43}$$

The nonlinear system is solved for the global d.o.f. vector $\mathbf{D}^g$ using the Newton–Raphson method in [8]. The convergence criterion is given by $\|\mathbf{R}^g\| \leq \epsilon_{tol}\|\mathbf{F}_{ex}^g\|$ and ϵ_{tol} is the prescribed tolerance, set to 10^{-4} in this work.

4. Numerical Investigation

Consider an FGP sandwich beam and an FGP sandwich frame made from SUS304 steel with pinned–pinned (PP) boundary conditions as illustrated in Figure 2. The temperature-dependent coefficients P_i $(i = -1, 0, 1, 2, 3)$ of the elastic modulus E, Poisson's ratio ν, and the thermal expansion coefficient λ for SUS304 are given in [5]. The geometric data are $L = 1$ m, $h = b = 0.05$ m, and $h_c/h_f = 8$. For convenience of discussion, the dimensionless parameters for the applied load and transverse displacement are defined as

$$u_0^* = \frac{u_0(\text{considered})}{h}, w_0^* = \frac{w_0(\text{considered})}{h}, \; P^* = \frac{PL^2}{E_1 I} \text{ with I} = \frac{bh^3}{12} \tag{44}$$

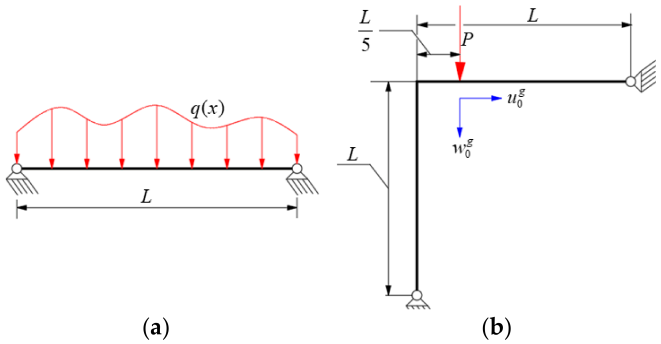


Figure 2. Beam and frame used in analysis. (**a**) Simply supported beam under distributed load q(x); (**b**) asymmetric frame under a concentrated load P. Red arrows indicate the applied loads, while blue arrows indicate the displacement components.

No studies on FGP sandwich frame problems considering thermal effects have been reported. Therefore, the present model is validated through comparison for special cases, especially the nonlinear bending response being compared with the result of Ref. [9]. Table 1 demonstrates the accuracy and convergence of the proposed element in predicting the dimensionless midspan deflection of an FGP beam under uniformly distributed load (UDL) and sinusoidally distributed load (SDL), using the above geometric parameters. For consistency, identical boundary conditions, material properties, and normalization are adopted. The parameters $E_1 = 200/(1 - v^2)$, $G_1 = 100/(1 + v_1)$, and $q_0 = 50 \times 10^3$ N/m are used. The error in Table 1 is defined as follows

$$\mathrm{Er}(\%) = \frac{\left|\mathrm{w}^*_{\mathrm{present}} - \mathrm{w}^*_{\mathrm{ref.}}\right|}{\mathrm{w}^*_{\mathrm{ref.}}} \times 100\% \tag{45}$$

where w^*_{present} and $w^*_{\mathrm{ref.}}$ are the dimensionless deflections from the present model and Ref. [9], respectively.

Table 1. Accuracy and convergence of w^* for a PP FGP beam under different distributed loads.

nELE	UDL			SDL		
	$e_0 = 0.25$	$e_0 = 0.50$	$e_0 = 0.75$	$e_0 = 0.25$	$e_0 = 0.50$	$e_0 = 0.75$
2	0.1151	0.1211	0.1277	0.0919	0.0967	0.1019
4	0.1150	0.1210	0.1276	0.0919	0.0966	0.1019
6	0.1150	0.1210	0.1276	0.0919	0.0966	0.1019
Ref. [9]	0.1133	0.1237	0.1307	0.0905	0.0953	0.1009
Er (%)	1.50%	2.18%	2.37%	1.55%	1.36%	0.99%

Table 1 confirms the good accuracy (Er < 2.4%) and rapid convergence (nELE ≥ 4) of the derived formulation. The deflection increases with e_0, indicating a reduction in stiffness. Moreover, UDL yields larger deflections than SDL, which is consistent with expected mechanical behavior and confirms the model.

Numerical Results

The nonlinear bending response of the FGP frame in thermal environment under a concentrated load P, as shown in Figure 2b, is analyzed and the results are depicted in Figure 3. Figure 3a shows the importance of the porosity distribution patterns on the nonlinear response, where the type I distribution yields the lowest displacements, while the type II gives the highest ones. One can conclude from Figure 3b that both the temperature and porosity coefficient significantly contribute to the deformation of the sandwich porous frames, and the increase in the coefficient e_0 or same temperature rise ΔT amplifies the dis-

placements. The amplification of the displacements becomes more significant by increasing both the temperature and porosity coefficient. A careful examination of Figure 3b shows that the effect of the temperature is more significant than that of the porosity coefficient.

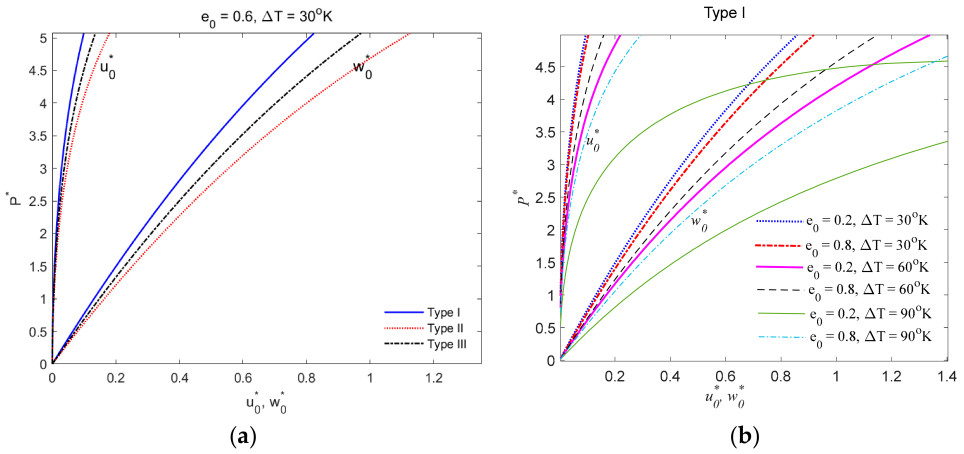


Figure 3. The nonlinear response of the FGP sandwich frame under thermomechanical loading with PP condition. (**a**) Effect of porosity distribution pattern; (**b**) effect of porosity and temperature variation.

Figure 4 shows the effect of boundary conditions on the nonlinear thermomechanical behavior of the FGP frame. The results indicate that the clamp–clamp (CC) frame is stiffer than the PP frame. As a result, the CC frame undergoes smaller displacements under the same loading conditions.

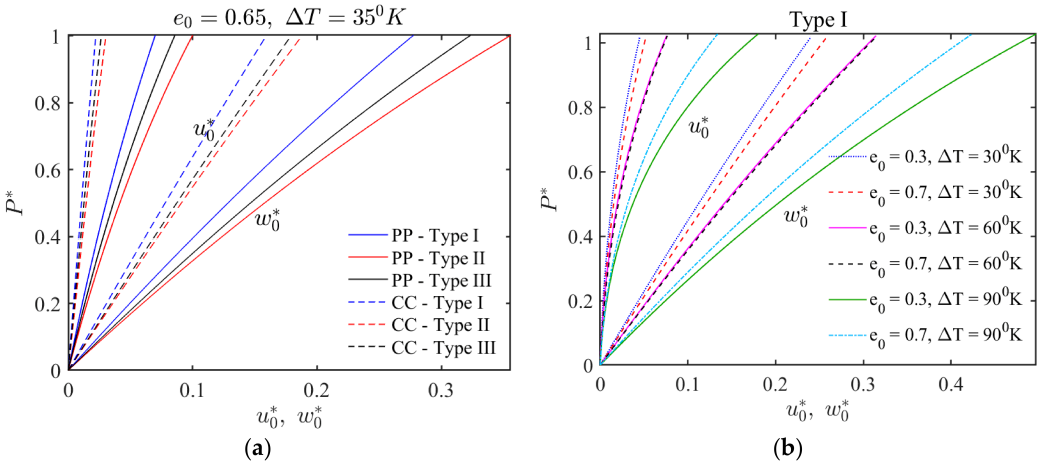


Figure 4. The nonlinear response of the FGP sandwich frame under thermomechanical loading with different boundary conditions. (**a**) Effect of porosity distribution pattern for PP and CC boundary conditions; (**b**) effect of porosity coefficient and temperature variation for type I porous distribution pattern for CC.

5. Conclusions

An efficient finite beam formulation for predicting the thermoelastic nonlinear bending of sandwich frames with an FGP core has been presented. The formulation incorporates temperature-dependent properties; graded porosity distributions are derived based on the third-order shear deformation theory and von Kármán nonlinearity. By adopting shear rotation as an independent variable, computational efficiency is improved, and the nonlinear problem is solved using the Newton–Raphson method. The results demonstrate the efficiency of the formulation and the strong impact of the temperature and porosity on

the nonlinear structural response. The deformation of the frames is significantly increased when increasing both the porosity coefficient and temperature.

Author Contributions: Writing-original draft, investigation, formal analysis, T.T.P.; methodology, conceptualization, supervision, D.K.N.; validation, writing-review and editing, C.I.L. All authors have read and agreed to the published version of the manuscript.

Funding: This research received no external funding.

Institutional Review Board Statement: Not applicable.

Informed Consent Statement: Not applicable.

Data Availability Statement: The original contributions presented in this study are included in the article. Further inquiries can be directed to the corresponding author.

Conflicts of Interest: The authors declare no conflicts of interest.

References

1. Chen, D.; Kitipornchai, S.; Yang, J. Nonlinear free vibration of shear deformable sandwich beam with a functionally graded porous core. *Compos. Struct.* **2016**, *163*, 311–325.
2. Shi, G.; Lam, K.Y.; Tay, T.E. On efficient finite element modeling of composite beams and plates using higher-order theories and an accurate composite beam element. *Compos. Struct.* **1998**, *41*, 159–165. [CrossRef]
3. Chen, D.; Yang, J.; Kitipornchai, S. Free and forced vibrations of shear deformable functionally graded porous beams. *Int. J. Mech. Sci.* **2016**, *108*, 14–22. [CrossRef]
4. Wattanasakulpong, N.; Ungbhakorn, V. Linear and nonlinear vibration analysis of elastically restrained ends FGM beams with porosities. *Aerosp. Sci. Technol.* **2014**, *32*, 111–120. [CrossRef]
5. Kim, Y.W. Temperature dependent vibration analysis of functionally graded rectangular plates. *J. Sound Vib.* **2005**, *284*, 531–549. [CrossRef]
6. Reddy, J.N. A simple higher-order theory for laminated composite plates. *J. Appl. Mech.* **1984**, *54*, 745–752. [CrossRef]
7. Crisfield, M.A. *Nonlinear Finite Element Analysis of Solids and Structures*; Wiley: New York, NY, USA, 1991.
8. Krenk, S. *Non-Linear Modeling and Analysis of Solids and Structures*; Cambridge University Press: Cambridge, UK, 2009.
9. Srikarun, B.; Songsuwan, W.; Wattanasakulpong, N. Linear and nonlinear static bending of sandwich beams with functionally graded porous core under different distributed loads. *Compos. Struct.* **2021**, *276*, 114538. [CrossRef]

Disclaimer/Publisher's Note: The statements, opinions and data contained in all publications are solely those of the individual author(s) and contributor(s) and not of MDPI and/or the editor(s). MDPI and/or the editor(s) disclaim responsibility for any injury to people or property resulting from any ideas, methods, instructions or products referred to in the content.